Journal of Nuclear Materials 457 (2015) 182–185

Contents lists available at ScienceDirect

Journal of Nuclear Materials

journal homepage: www.elsevier.com/locate/jnucmat

Grain size effects on He bubbles distribution and evolution

J. Wang [a,b,c], X. Gao [a], N. Gao [a], Z.G. Wang [a,*], M.H. Cui [a], K.F. Wei [a], C.F. Yao [a], J.R. Sun [a], B.S. Li [a], Y.B. Zhu [a], L.L. Pang [a], Y.F. Li [a,b,c], D. Wang [a,b], E.Q. Xie [c]

[a] Institute of Modern Physics, Chinese Academy of Sciences, Lanzhou 730000, China
[b] University of Chinese Academy of Sciences, Beijing 100049, China
[c] School of Physical Science and Technology, Lanzhou University, Lanzhou 730000, China

HIGHLIGHTS

- SMAT treated T91 and conventional T91 were implanted by 200 keV He^{2+} to 1×10^{21} He m^{-2} at room temperature and annealed at 450 °C for 3.5 h.
- He bubbles in nanometer-size-grained T91 are smaller in as-implanted case.
- The bubbles in the matrix of nanograins were hard to detect and those along the nanograin boundaries coalesced and filled with the grain boundaries after annealing.
- Brownian motion and coalescence and Ostwald ripening process might lead to bubbles morphology presented in the nanometer-size-grained T91 after annealing.

ARTICLE INFO

Article history:
Received 29 April 2014
Accepted 7 November 2014
Available online 15 November 2014

ABSTRACT

Grain boundary and grain size effects on He bubble distribution and evolution were investigated by He implantation into nanometer-size-grained T91 obtained by Surface Mechanical Attrition Treatment (SMAT) and the conventional coarse-grained T91. It was found that bubbles in the nanometer-size-grained T91 were smaller than those in the conventional coarse-grained T91 in as-implanted case, and bubbles in the matrix of nanograins were undetectable while those at nanograin boundaries (GBs) coalesced and filled in GBs after heat treatment. These results suggested that the grain size of structural material should be larger than the mean free path of bubble's Brownian motion and/or denuded zone around GBs in order to prevent bubbles accumulation at GBs, and multiple instead of one type of defects should be introduced into structural materials to effectively reduce the susceptibility of materials to He embrittlement and improve the irradiation tolerance of structural materials.

1. Introduction

Large number of helium atoms will be introduced into structural materials via either (n, α) transmutation reactions or by direct injection in the future advanced fusion and fission reactors. The very low solubility and low migration energy (0.078 eV) of He atoms in steels [1] indicate that the helium atoms are easy to aggregate into helium bubbles, He–vacancy clusters at different kinds of sinks, such as dislocations, grain boundaries, and surfaces of precipitates [2–7]. Once the size of bubbles is larger than a critical radius, they would have obvious detrimental effects on material properties, e.g. He-induced embrittlement, swelling *etc*. This has been considered as one of the critical issues for structural materials during a reactor's operational lifetime. As a result, the availability and mobility of He atoms must be managed in ways that growth of He bubbles is suppressed so as to mitigate the susceptibility of these alloys to He embrittlement.

Among the many new ways to suppress He bubbles growth, increasing the density of defects acting as sinks for helium atoms has been proved to be an effective way [8–14]. For instance, a large quantity of nanometer-size particles have been introduced to oxide dispersion strengthened (ODS) steels as He trapping and nucleation sites [12–14]. Except the nanometer-size particles, grain boundaries could also act as trapping and nucleation sites and have attracted considerable attention. For example, the simulations performed by Bai et al. suggested the grain boundaries as possible sinks for irradiation induced defects [15]. Ackland also suggested the way of controlling radiation damage by increasing the number density of grain boundaries [16] based on recent published work. In addition, due to the excellent mechanical properties of nanocrystalline (NC) alloys, NC alloys have also been tested for their

* Corresponding author.
E-mail address: zhgwang@impcas.ac.cn (Z.G. Wang).

http://dx.doi.org/10.1016/j.jnucmat.2014.11.036
0022-3115/

irradiation-resistant properties since Gleither first presented the concepts of nanocrystalline material [17]. The superior radiation tolerance of nanostructured ferritic alloys (NFAs) with dispersed nanometer-size oxides [3,18,19] has then been demonstrated experimentally. More recent studies by Moslang et al. [3] and subsequent work by Edmondson et al. [4–6] verified the hypothesis that the surfaces of nanoclusters in NFAs are the preferential nucleation sites for He bubbles formation. However, He bubbles evolution at nanograin boundaries and inside of the nanograin of NC alloys have not been studied in detail. In this study, we will focus on this issue with the help of Surface Mechanical Attrition Treatment (SMAT) technique which could provide us refined grain into the nanometer scale in the surface layer of bulk materials without changing their chemical composition [20]. It is noted that the nanograins induced by SMAT have been proved to be stable below 500 °C in ferritic steels [21]. Thus, He bubbles behavior at nanograin boundaries and inside of the nanograin could be explored.

Commercial ferritic/martensitic steel T91 was chosen to be investigated in the present work due to the maturity in industrial production and its important applications in nuclear reactors. Both SMAT treated and untreated samples were irradiated by He^{2+} ions to fluence of 1×10^{21} ions m^{-2} at room temperature. The bubble size and number distribution in nanometer-size-grained T91 (SMAT treated) and coarse-grained T91 (without SMAT treated) have been analyzed statistically.

2. Experiment details

The chemical composition of T91 is listed in Table 1. The samples were normalized at 1050 °C for 20 min and tempered at 780 °C for 60 min. The size of the samples is $9 \times 9 \times 5$ mm^3. They were firstly well mechanically polished until mirror-like surfaces formed. In order to get nanometer scale grains, those samples were treated by the technique of SMAT. The SMAT treated samples were then annealed at 300 °C for 3 h with a vacuum state of 10^{-5} Pa to remove the residual stress induced during the SMAT process. The cross-sectional micrograph of as treated T91 sample around the depth of peak He concentration is presented in Fig. 1.

SMAT treated T91 samples were then irradiated with 200 keV He ions at room temperature to fluence of 1×10^{21} ions m^{-2} at a terminal chamber of the 320 kV multi-discipline research platform for highly charged ions at the Institute of Modern Physics (IMP) in Lanzhou, China. Ion beam was scanned to a homogeneous distribution of 12×12 mm^2 to keep the uniformity of irradiation fluence. Due to the ion beam heating effect, the intensity of ion beam was controlled purposely and specimens were mounted on a large steel block using copper tape to ensure good thermal conductivity so that temperature was controlled below 50 °C which was measured by infrared thermometer. For comparison, the well mechanically polished T91 samples with the same annealing heat treatment but without SMAT treated were irradiated under the same condition. According to the calculation with Stopping and Range of Ions in Matter (SRIM) 2011.08 code in full cascade mode [22], the peak He concentration with value of ~5.9 at.% is located at a depth of ~540 nm and the FWHM of the He concentration peak is 175 nm. The irradiated samples were then annealed at 450 °C for 3.5 h at a vacuum state of 10^{-5} Pa. As the 200 keV He implantation resulted in a highly non-uniform implantation profile in vertical direction, cross-sectional TEM specimens were prepared accordingly. The cross-sectional TEM specimens were first mechanically polished down to a thickness of ~20 μm, then ion milling in a Gatan precision ion polishing system with Ar beam energies of 5 keV gradually decreasing to 3 keV was employed to obtain the specimen with thickness that is transparent for electrons. The TEM samples were analyzed in a FEI-TF20 transmission electron microscope operating at 200 keV.

Table 1
Chemical composition (wt.%) of T91.

C	Mn	P	S	Si	Cr
0.095	0.46	0.012	0.0008	0.26	8.45
Nb	V	Al	Ni	Mo	
0.075	0.20	0.01	0.17	0.92	

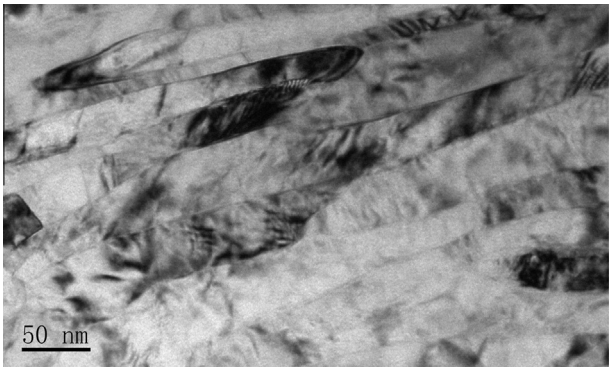

Fig. 1. TEM micrograph of SMAT T91 before irradiation recorded in the regions of He deposition.

3. Results and discussions

Among the factors that affect He bubbles behavior in steels, local microstructure plays a key role in He trapping and bubbles nucleation. In the refined grain layer of SMAT steels, the width of lath-like grains increase from ~10 nm near the surface to more than 100 nm at a depth of about 30 μm [20,21,23,24]. When the energy of He ions was chosen to be 200 keV, the corresponding peak of He concentration curve is located around 540 nm with FWHM of 175 nm. The cross-sectional TEM micrograph of the sample at the same depth before the irradiation is shown in Fig. 1. From Fig. 1, it can be found that the coarse grains before SMAT changed to the lath-like grains with width ranging from ~20 nm to ~50 nm. The explanation of such change can be found in the Refs. [20,21,23,24].

The typical morphology of He bubbles in regions of the highest He concentration in nanometer-size-grained T91 and its coarse-grained counterpart in as-implanted case are shown in Fig. 2a and b, respectively. The size of bubbles in the nanometer-size-grained T91 is smaller than the bubbles in coarse-grained T91 as shown in Fig. 2. From Fig. 2a, it can be observed that the helium bubbles nucleated at the grain boundaries are bigger and denser than bubbles in the nanograin matrix. The results from Fig. 2b indicate a relatively non-uniform size distribution of bubbles in coarse grained T91 and these bubbles are generally larger than those bubbles in SMAT treated T91. In order to make a quantitative comparison, statistics on bubble size were made for both samples. In this work, minimum discernable bubble diameter was 0.8 nm. The statistic of the size and number of visible bubbles along the GBs and in matrix were made in a rectangular region. The rectangular region was defined with width equaling to the width of the helium deposition band area and length of 500 nm along the He deposition band in the cross sectional TEM image. The corresponding histograms of the bubble size distribution in the nanograins and coarse grains are shown in Fig. 3. Bubbles in the matrix of coarse grains untreated have a mean diameter of ~2.20 nm, while bubbles along nanograin boundaries and inside the nanograins have a mean diameter of ~2.11 nm and ~1.88 nm, respectively. For bubbles in